Journal of Catalysis 274 (2010) 287–295

Contents lists available at ScienceDirect

Journal of Catalysis

journal homepage: www.elsevier.com/locate/jcat

Aqueous-phase reforming of ethylene glycol to hydrogen on Pd/Fe_3O_4 catalyst prepared by co-precipitation: Metal–support interaction and excellent intrinsic activity

Jun Liu [a], Bo Sun [a], Jiye Hu [a], Yan Pei [a], Hexing Li [b], Minghua Qiao [a,*]

[a] Department of Chemistry and Shanghai Key Laboratory of Molecular Catalysis and Innovative Materials, Fudan University, Shanghai 200433, PR China
[b] Department of Chemistry, Shanghai Normal University, Shanghai 200234, PR China

ARTICLE INFO

Article history:
Received 14 May 2010
Revised 9 July 2010
Accepted 14 July 2010
Available online 11 August 2010

Keywords:
APR
Pd/Fe_3O_4
Co-precipitation
Ethylene glycol
H_2

ABSTRACT

A high-performance Pd/Fe_3O_4 catalyst for aqueous-phase reforming (APR) of ethylene glycol (EG) to H_2 was prepared facilely by the co-precipitation method. After proper activation, the Pd was present as highly dispersed metallic nanoparticles with dimension of <3 nm, and the Fe was present as magnetite. When compared to Pd catalyst supported on Fe_2O_3, NiO, Cr_2O_3, Al_2O_3, or ZrO_2 prepared by incipient wetness impregnation, the Pd/Fe_3O_4 catalyst displayed superior catalytic performance in terms of activity, selectivity, and stability. The intrinsic activity of the Pd/Fe_3O_4 catalyst was about three times of that of the second most active Pd/Fe_2O_3 catalyst under the same reaction conditions. In addition, the Pd/Fe_3O_4 catalyst retained ~80% of its initial activity after reaching the steady-state. Notably, the Pd/Fe_3O_4 catalyst possessed the highest turnover frequency of H_2 (109 min^{-1}) reported so far, showing its promise as a new practical catalyst for APR of biomass-derived oxygenates to H_2. The excellent catalytic performance of the Pd/Fe_3O_4 catalyst was attributed to the enhanced synergistic effect between small Pd nanoparticles and magnetite in promoting the water–gas shift reaction, the rate-determining step in APR of EG over Pd-based catalysts.

1. Introduction

Hydrogen is a clean fuel that emits only water when combusted or used in polymer electrolyte membrane fuel cells. However, the production of H_2 nowadays is far from clean. Approximately 95% of H_2 is produced from carbonaceous fossil fuels, which inevitably results in tremendous CO_2 emissions. Greener production routes of H_2 from water by solar- or wind-driven electrolysis and photo-biological water splitting, however, are less competitive due to the present-day high costs to utilize these renewable energies [1–3]. Therefore, much attention has been paid to the production of H_2 from biomass, which in principle leads to net zero CO_2 emissions [4]. Among these endeavors, Dumesic and coworkers demonstrated that the catalytic aqueous-phase reforming (APR) of biomass-derived oxygenates such as glucose, sorbitol, glycerol, and ethylene glycol (EG) is thermodynamically and kinetically feasible in generating H_2-rich fuel gas [5–8]. The APR process is promising owing to its advantages of higher energy efficiency and lower CO concentration in the product gas than the conventional steam reforming processes [9].

The mechanism of H_2 production from APR of EG has been described in the literature [10]. According to that mechanism, a good APR catalyst should not only be active for the cleavage of the C–C bond but also be active for the water–gas shift (WGS) reaction [11]. Moreover, the catalyst should be inert to parallel and series competing reactions such as the cleavage of the C–O bond and the methanation reaction which greatly deteriorate the productivity of H_2. Based on the works of Sinfelt and Yates [12] and Grenoble et al. [13], Davda et al. deduced that Pt and Pd could meet these criteria and would be promising catalysts for APR of EG to H_2 [7]. It was verified that the Pt/Al_2O_3 catalyst is both active and selective in APR of EG to H_2 [5]. On the other hand, although the Pd/SiO_2 catalyst is also highly selective to H_2, its activity expressed in terms of the rate of CO_2 production is about one order of magnitude inferior to that of the Pt/SiO_2 catalyst [7]. Since the rate of the WGS reaction over Pd catalysts is lower than that over Pt catalysts, while the rate of C–C bond cleavage in ethane hydrolysis is similar for Pd- and Pt-based catalysts, Huber et al. deduced that the rate-determining step for APR of EG on Pd could be the WGS reaction [9].

The activity of the supported catalysts critically depends both on the metal and on the support itself [14], and high-performance catalyst can be designed by taking into account the significant contribution of the support [15,16], which is also true for the

* Corresponding author. Fax: +86 21 65641740.
E-mail address: mhqiao@fudan.edu.cn (M. Qiao).

0021-9517/$ - see front matter © 2010 Elsevier Inc. All rights reserved.
doi:10.1016/j.jcat.2010.07.014

APR catalyst. By supporting Pd on Fe_2O_3 (Nanocat) using incipient wetness impregnation (IWI), Huber et al. found that the production rates of CO_2 and H_2 were surprisingly elevated to about 10 times higher than those on the Pt/Al_2O_3 catalyst [9]. Because Fe_2O_3 did not promote the WGS activity of Pt [9] and vice versa [17], and Pd/Fe_2O_3 catalysts were several orders of magnitude more active than the Pd/SiO_2 catalyst for WGS [18], Huber et al. concluded that the high activity of the Pd/Fe_2O_3 catalyst in APR of EG was caused by the synergistic combination of Pd and Fe_2O_3 which boosts the WGS reaction [9]. However, it is unfortunate that the Pd/Fe_2O_3 catalyst lost 50% of its activity after being heated to 483 K under APR reaction conditions.

Enlightened by these works, we suggest that if a more intimate interaction between Pd and iron oxide can be achieved, in principle the synergistic effect could be enhanced further, and an even more active and stable iron oxide-supported Pd catalyst could be developed. Following this idea, in this work we prepared a Pd/Fe_3O_4 catalyst using the co-precipitation method which usually leads to a better interaction between metal and support than the impregnation method [19–22] and evaluated its catalytic performance in APR of EG to H_2. Although the APR performance of the Pd/Fe_2O_3 catalyst prepared by IWI has been investigated previously [9], this catalyst was not fully characterized. So, in the present work we also prepared the Pd/Fe_2O_3 catalyst by IWI and systematically characterized and evaluated this catalyst for the purpose of comparison. The excellent catalytic performance of the Pd/Fe_3O_4 catalyst was discussed and correlated with the characterization results.

2. Experimental

2.1. Catalyst preparation

The Pd/Fe_3O_4 catalyst was prepared by the co-precipitation method [23]. Under stirring, 4.1 g of $Fe(NO_3)_3{\cdot}9H_2O$ was dissolved in 14 ml of $PdCl_2$ solution (3.2×10^{-2} M) at room temperature. Then, 30 ml of Na_2CO_3 solution (1.0 M) was added dropwise to the mixed solution, and the pH of the final solution was ca. 8.5. After stirring and standing for 3 h respectively, the resulting precipitate was filtered, washed with deionized water several times, air-dried at 373 K overnight, and calcined in air at 573 K for 3 h. The resulting brown powder was denoted as $Pd/Fe(OH)_x$. Prior to activity testing and characterizations, the $Pd/Fe(OH)_x$ precursor was reduced in 5 vol.% H_2/Ar (50 ml min^{-1}) at 473 K for 3 h at a heating rate of 1 K min^{-1}. The as-reduced catalyst was denoted as Pd/Fe_3O_4.

The Pd/Fe_2O_3 catalyst was prepared by the IWI method. Fe_2O_3 was prepared by thermal decomposition of $Fe(NO_3)_3{\cdot}9H_2O$ at 673 K. Then, 4.2 ml of $PdCl_2$ solution (0.11 M) was impregnated onto 1.0 g of the as-prepared Fe_2O_3 and stayed at room temperature overnight, followed by drying at 373 K overnight and calcination at 573 K for 2 h. The Al_2O_3- (Shanghai Super), ZrO_2-, Cr_2O_3-, and NiO-supported (Shanghai Chemical Reagents) Pd catalysts were also prepared by IWI to expand our study on the effect of support on the APR performance of Pd. These catalyst precursors were reduced similarly to that of Pd/Fe_3O_4. The nominal Pd loading was fixed at 5.0 wt.% on all the supports, and the practical Pd loading in all the reduced catalysts was in the range of 4.7 ± 0.1 wt.%, as determined by inductively coupled plasma–atomic emission spectroscopy (ICP–AES, IRIS Intrepid). The amount of Na retained in the Pd/Fe_3O_4 catalyst was ~1 ppm. So, the influence of Na on the reactivity of the Pd/Fe_3O_4 catalyst should be minimal, if any.

2.2. Catalyst characterization

Powder X-ray diffraction (XRD) was executed on a Bruker AXS D8 Advance X-ray diffractometer in a step mode using Cu Kα radiation (0.15418 nm). The X-ray tube was operated at 40 kV and 40 mA. The mean crystallite size of Fe_3O_4 was calculated from the full width at the half maximum (FWHM) of the Fe_3O_4(3 1 1) diffraction peak according to the Scherrer equation.

Temperature programmed reduction (TPR) was carried out on a home-made apparatus. About 50 mg of the catalyst precursor was degassed at 473 K under Ar for 2 h. After cooling down to room temperature in the blanket of Ar, the gas was switched to 5 vol.% H_2/Ar (50 ml min^{-1}), and the sample was heated to 873 K at a ramping rate of 10 K min^{-1}. The amount of H_2 consumed was monitored by a thermal conductivity detector (TCD).

The Brunauer–Emmett–Teller (BET) surface area (S_{BET}) and porosity were acquired by N_2 physisorption at 77 K on a Micromeritics TriStar3000 apparatus. The microstructure was observed on a JEOL JEM 2011 transmission electron microscope (TEM) operating at 200 kV.

The active surface area (S_{act}) was measured based on CO desorption. To remove H_2 adsorbed on the catalyst reduced in H_2/Ar, the catalyst was heated at 498 K in Ar (deoxygenated by an Alltech Oxy-trap filter) for 1 h. After the catalyst was cooled down to room temperature under Ar, CO pulses were injected until the eluted peak areas of consecutive pulses were constant. The maximum desorption temperature, 973 K, was achieved at a heating rate of 10 K min^{-1}. S_{act} was calculated from the volume of CO desorbed by assuming CO/Pd_s stoichiometry of 1 and a surface area of 7.87×10^{-20} m^2 per Pd atom [24].

The surface chemical state was determined by X-ray photoelectron spectroscopy (XPS, Perkin–Elmer PHI5000C) using Mg Kα radiation (1253.6 eV). The catalyst covered by ethanol was mounted on the sample plate, degassed in the pretreatment chamber at 393 K for 4 h in vacuo, and then transferred to the analyzing chamber where the background pressure was $<2 \times 10^{-9}$ Torr. All binding energy (BE) values were calibrated by C 1s peak of contaminant carbon at 284.6 eV with an uncertainty of ±0.2 eV.

2.3. Activity testing

The reactor system for APR of EG was established according to the set-up described by Shabaker et al. [10]. The catalyst precursor (~1.30 g for $Pd/Fe(OH)_x$ and 1.06 g for others) was loaded in the stainless steel tubular reactor (i.d. 6 mm) and reduced on site with 5 vol.% H_2/Ar at 473 K for 3 h, followed by cooling down to 303 K under the same atmosphere before exposure to an aqueous solution of 5.0 wt.% EG. Argon was used to regulate the system pressure. The reforming was typically conducted with catalyst containing 0.05 g of Pd, weight hourly space velocity (WHSV (weight flow rate of the feed solution) × (weight fraction of EG in the feed)/(weight of Pd in the catalyst)) of 3.6 h^{-1}, temperature of 498 K, and system pressure of 2.58 MPa, unless otherwise specified. The stability test was conducted under above reaction conditions up to 130 h on stream.

During the reaction, the gas products were analyzed by an online gas chromatograph (GC122). H_2, CO, CH_4, and CO_2 were separated by a 2-m TDX-01 packed column and examined by TCD. Methane, ethane, propane, and butane were separated by a DM PoraPlot Q capillary column (10 m × 0.53 mm × 20 μm) and examined by a flame ionization detector (FID). Liquid phase effluent was condensed and analyzed gas chromatographically using the same capillary column and FID detector. The liquid products were also qualified by GC-MS (Finnigan Voyager) fitted with an HP-5 capillary column. The carbon balance was within ±5% for all the catalytic runs, indicating negligible carbon deposition on the Pd/Fe_3O_4 catalyst.

According to Shabaker et al. [25], the selectivity to H_2 was defined as:

$$H_2\ \text{selectivity}\ (\%) = [(\text{moles of } H_2 \text{ produced})/(\text{moles of C in gas phase})] \times (2/5) \times 100$$

which takes into account of the occurrence of the WGS reaction; and the selectivity to alkane was defined as:

$$\text{Alkane selectivity}\ (\%) = [(\text{moles of C in gaseous alkanes})/(\text{total moles of C in gas products})] \times 100$$

According to these definitions, the summation of the selectivities to H_2 and alkane does not lead to unity, for they were calculated based on independent hydrogen and carbon balances, respectively.

3. Results and discussion

3.1. Physicochemical properties

Fig. 1 shows the XRD patterns of the Pd/Fe(OH)$_x$ precursor, the corresponding Pd/Fe_3O_4 catalyst, Fe(OH)$_x$ prepared in the way similar to that of the Pd/Fe(OH)$_x$ precursor but in the absence of $PdCl_2$ and subjected to the same reduction treatment as Pd/Fe(OH)$_x$ (abbreviated as Fe(OH)$_x$–R), Fe_2O_3 without supporting of Pd, as well as the Pd/Fe_2O_3 catalyst. It is interesting that no diffraction peak could be detected for the Pd/Fe(OH)$_x$ precursor, indicating that Fe(OH)$_x$ was in the amorphous state, and PdO was highly dispersed with the crystallite size beyond the detection limit of XRD. After reduction, weak diffraction peaks of magnetite (Fe_3O_4, JCPDS 85–1436) emerged for the Pd/Fe_3O_4 catalyst. In contrast, there were only diffraction peaks ascribable to hematite (α-Fe_2O_3, JCPDS 85–0986) for Fe(OH)$_x$–R, indicating that Pd was so active that Fe(OH)$_x$ could be reduced to magnetite at 473 K. No diffraction peaks of maghemite (γ-Fe_2O_3, JCPDS 39–1346) such as (1 1 0), (2 1 0), and (2 1 1) reflections, which are stronger than the γ-Fe_2O_3(1 1 1) reflection at the same position of the Fe_3O_4(3 1 1) reflection, were observed for the Pd/Fe_3O_4 catalyst, indicating the exclusive transformation of Fe(OH)$_x$ to magnetite. Based on the Scherrer equation and the most intensive Fe_3O_4(3 1 1) diffraction peak, the average crystallite size of magnetite was estimated to be ca. 11 nm. Again, no diffraction peaks of metallic Pd were discernable, indicating that Pd remained highly dispersed in the Pd/Fe_3O_4 catalyst after reduction.

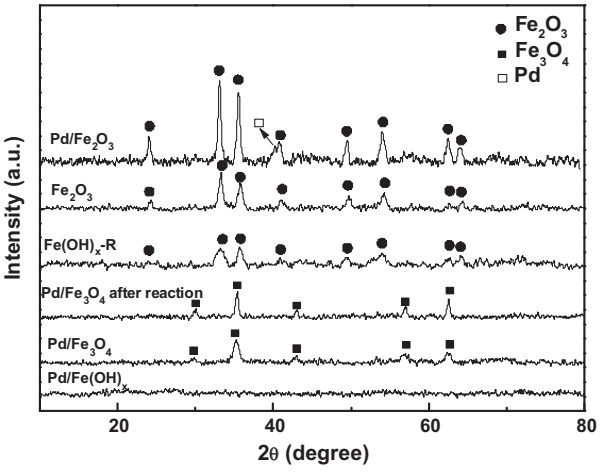

Fig. 1. XRD patterns of the Pd/Fe(OH)$_x$ precursor, the Pd/Fe_3O_4 catalyst before and after 130 h on stream in APR of 5 wt.% EG at 498 K, 2.58 MPa, and WHSV of 3.6 h^{-1}, Fe(OH)$_x$ prepared in the way similar to that of the Pd/Fe(OH)$_x$ precursor but in the absence of $PdCl_2$ and subjected to the same reduction treatment as Pd/Fe(OH)$_x$ (abbreviated as Fe(OH)$_x$–R), Fe_2O_3 without supporting of Pd, and the Pd/Fe_2O_3 catalyst.

The XRD pattern of the Pd/Fe_2O_3 catalyst prepared by IWI clearly presents diffraction peaks at 2θ of 24.0°, 33.1°, 35.5°, 40.8°, 49.5°, 53.9°, 62.4°, and 64.0° ascribable to hematite. However, the appearance of small features at 2θ of 30.0°, 43.0°, and 56.9° and the lowered (1 0 4)/(1 1 0) and improved (2 1 4) to (3 0 0) intensity ratios with respect to those of the standard diffractogram of hematite strongly indicate the presence of a small amount of magnetite in this catalyst, although the H_2–TPR result presented below showed that this reduction temperature was not sufficient to transform bulk hematite to magnetite. Compared with the XRD pattern of Fe_2O_3 without supporting of Pd, the strongest (1 1 1) reflection of metallic Pd at 2θ of ca. 40.2° was readily discerned on this catalyst, which evidences that the crystallite size of metallic Pd was larger than that in the Pd/Fe_3O_4 catalyst, inferring that the interaction between Pd and iron oxide in the Pd/Fe_3O_4 catalyst prepared by co-precipitation is much stronger than that in the Pd/Fe_2O_3 catalyst prepared by IWI.

The H_2–TPR profiles of Pd/Fe(OH)$_x$ and Pd/Fe_2O_3 precursors are shown in Fig. 2. For comparison, the reduction profiles of hematite without supporting of Pd as well as Fe(OH)$_x$ are also presented. Fe(OH)$_x$ showed two broad H_2 consumption peaks at ~694 K and 890 K. After incorporation of Pd into Fe(OH)$_x$, the peak at ~694 K disappeared, and a broad peak centered at ~430 K emerged. Since the XRD pattern of the Pd/Fe_3O_4 catalyst reduced at 473 K indicated the formation of magnetite, the H_2 consumption peak at ~430 K was assigned to the simultaneous reduction of Pd^{2+} to metallic Pd and Fe(OH)$_x$ to magnetite. The high-temperature H_2 consumption peak is therefore assigned to the reduction of magnetite to wüstite and metallic iron [26]. Considering the fact that the peak areas of the low-temperature H_2 consumption peaks of the Pd/Fe(OH)$_x$ precursor and Fe(OH)$_x$ are similar, the H_2 consumption peak at 694 K for Fe(OH)$_x$ is assigned to the transition to magnetite accordingly.

In the H_2–TPR profiles of hematite and the Pd/Fe_2O_3 precursor, the first H_2 consumption peak was found at 675 K for hematite and at 575 K for the Pd/Fe_2O_3 precursor, showing that Pd is also effective in promoting the reduction of hematite to magnetite. A similar decrement in the reduction temperature of hematite has been observed by Chang et al. on the Au/Fe_2O_3, Ru/Fe_2O_3, and Au–Ru/Fe_2O_3 catalysts prepared by deposition–precipitation [27]. The small H_2 consumption peak at 451 K for the Pd/Fe_2O_3 precursor can be attributed to the reduction of Pd^{2+} to metallic Pd based on the area of this peak. Musolino et al. prepared a Pd/Fe_2O_3 precursor with the same Pd loading and method and found that the reduction temperature of hematite to magnetite was virtually identical to our

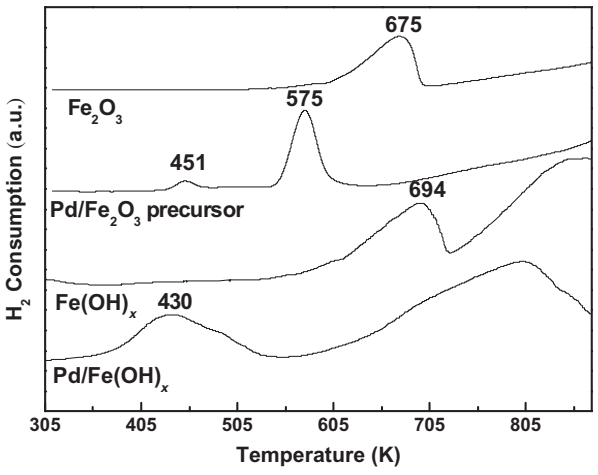

Fig. 2. H_2–TPR profiles of the Pd/Fe(OH)$_x$ precursor, Fe(OH)$_x$, the Pd/Fe_2O_3 precursor, and hematite.

observation [28]. However, they observed a lower reduction temperature of Pd^{2+} to metallic Pd (ca. 360 K), which is probably a result of changes in palladium salt and thermal treatment conditions. The more drastic decrement in the reduction temperature of ferric ions to magnetite in $Fe(OH)_x$ (ΔT = 264 K) than in Fe_2O_3 (ΔT = 100 K) in the presence of Pd is a clear sign of the much stronger interaction between Pd species and iron oxide in the $Pd/Fe(OH)_x$ precursor than in the Pd/Fe_2O_3 precursor.

Fig. 3 shows the N_2 isotherms and pore size distribution (PSD) curves of the Pd/Fe_3O_4 and Pd/Fe_2O_3 catalysts. Notably, the Pd/Fe_3O_4 catalyst exhibited a type IV isotherm and a type H2 hysteresis loop at the relative pressure range of 0.5–0.8, which is characteristic of a mesoporous structure [29]. The corresponding PSD curve displayed a relatively uniform pore size centered at ca. 3.4 nm. However, for the Pd/Fe_2O_3 catalyst the hysteresis loop was shifted to higher relative pressure, indicating the existence of larger pores as confirmed by its corresponding PSD curve.

As summarized in Table 1, the BET surface areas of the $Pd/Fe(OH)_x$ precursor and $Fe(OH)_x$ were 229 and 110 $m^2\,g^{-1}$, respectively, which were much larger than the values of 18 and 23 $m^2\,g^{-1}$ of the Pd/Fe_2O_3 precursor and hematite. It is remarkable that the S_{BET} of the $Pd/Fe(OH)_x$ precursor was about two times of that of $Fe(OH)_x$ prepared in the same manner, showing that $PdCl_2$ also effectively improves the dispersion of $Fe(OH)_x$. In TEM images of $Fe(OH)_x$ and the $Pd/Fe(OH)_x$ precursor (not shown), the better dispersion of the nanoparticles in the latter is readily observed. After reduction, the S_{BET} of the Pd/Fe_3O_4 catalyst was slightly decreased to 190 $m^2\,g^{-1}$, which was close to the value of 170 $m^2\,g^{-1}$ for a similarly prepared Pd/Fe_3O_4 catalyst by Musolino et al. [28], but still being one order of magnitude larger than that of the Pd/Fe_2O_3 catalyst (17 $m^2\,g^{-1}$).

The TEM image in Fig. 4a shows that the particle size of magnetite in the Pd/Fe_3O_4 catalyst was mainly around 20 nm, and magnetite particles were uniform in size and well dispersed. In contrast, only after close inspection one can find uniform and small Pd nanoparticles highly dispersed on magnetite, as indicated by the arrows drawn in Fig. 4a. Fig. 4b shows the HRTEM image of the Pd/Fe_3O_4 catalyst, in which interplanar spacing of 0.22 nm corresponding to the (1 1 1) plane of *fcc* Pd (JCPDS 46–1043) was observed, and Pd nanoparticle with dimension of less than 3 nm was clearly identified, which accounts for the absence of the diffraction peaks of metallic Pd for the Pd/Fe_3O_4 catalyst. The interplanar spacing of 0.24 nm in Fig. 4b corresponds well to the (3 1 1) plane of magnetite [23]. For the Pd/Fe_2O_3 catalyst, Fig. 4c shows that hematite had much larger dimension of about 16 nm and broad particle size distribution (standard deviation of ±3 nm), and Pd nanoparticles had a dimension of about 10 nm and tended to aggregate.

Table 1
Physicochemical properties of $Fe(OH)_x$ and Fe_2O_3 supports, $Pd/Fe(OH)_x$ and Pd/Fe_2O_3 precursors, and Pd/Fe_3O_4 and Pd/Fe_2O_3 catalysts.

Sample	S_{BET} ($m^2\,g^{-1}$)	V_{pore} ($cm^3\,g^{-1}$)	d_{pore} (nm)	S_{act}[a] ($m^2\,g^{-1}$)
$Fe(OH)_x$	110	0.16	3.9	–
$Pd/Fe(OH)_x$	229	0.24	3.6	–
Pd/Fe_3O_4	190	0.20	3.3	4.0
Fe_2O_3	23	0.13	16.4	–
Pd/Fe_2O_3 precursor	18	0.067	11.4	–
Pd/Fe_2O_3	17	0.057	12.0	2.1

[a] Calculated from the amount of CO desorbed after saturation adsorption of CO.

3.2. APR of EG to H_2

Fig. 5 compares the catalytic activities in terms of the turnover frequencies (TOFs) of CO_2 over the Pd/Fe_2O_3, Pd/NiO, Pd/Cr_2O_3, Pd/Al_2O_3, and Pd/ZrO_2 catalysts prepared by IWI. The conversions of EG to gas products over these catalysts were all below 7.5%. It is evident that the Pd/Fe_2O_3 catalyst is intrinsically the most active one among the catalysts prepared by IWI. The activities of the Pd/Cr_2O_3 and the Pd/NiO catalysts were about one-sixth of that of the Pd/Fe_2O_3 catalyst. When Al_2O_3 and ZrO_2 were used as supports, the activities were further decreased by about one order of magnitude, which may be ascribed to the absence of synergistic effect between Pd and the support in these catalysts [11,30].

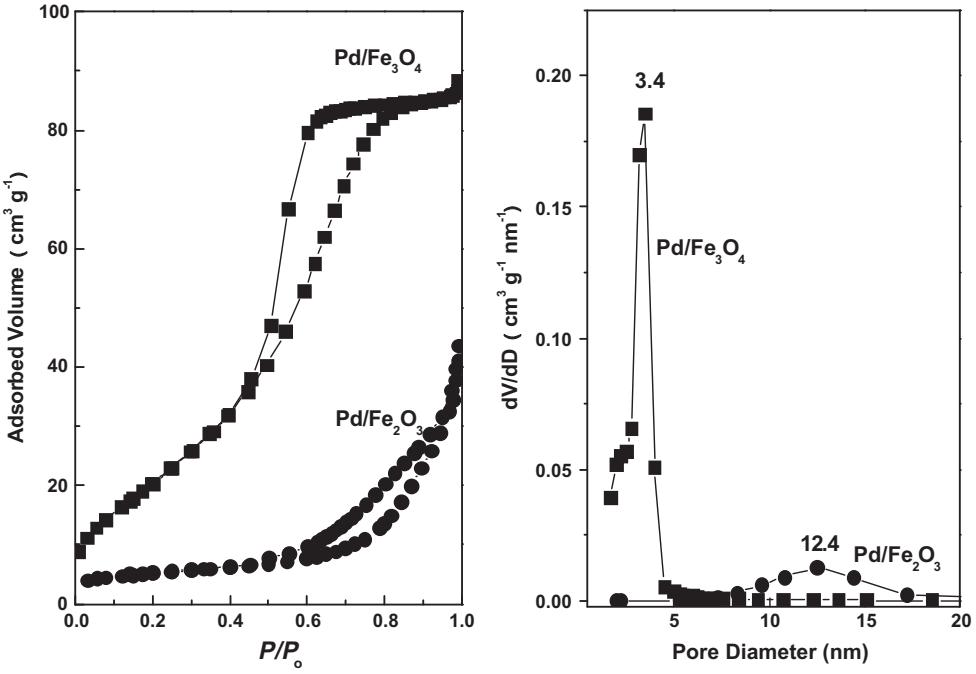

Fig. 3. N_2 adsorption–desorption isotherms and pore size distribution curves of the Pd/Fe_3O_4 and Pd/Fe_2O_3 catalysts.

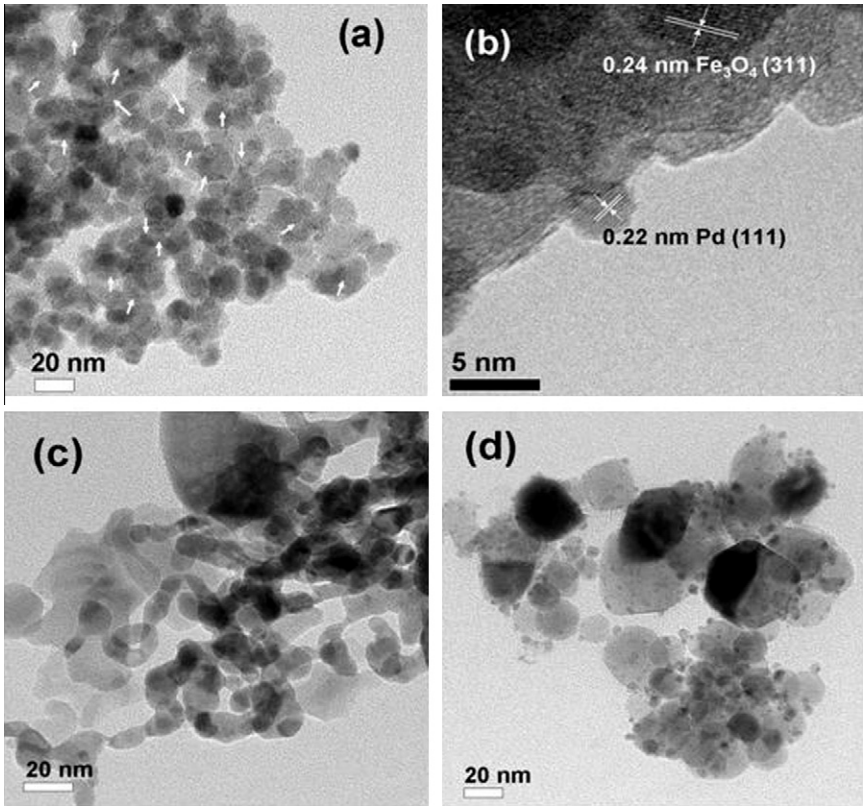

Fig. 4. TEM image (a) and HRTEM image (b) of the Pd/Fe_3O_4 catalyst, and TEM images of (c) the Pd/Fe_2O_3 catalyst and (d) the Pd/Fe_3O_4 catalyst after 130 h on stream in APR of 5 wt.% EG at 498 K, 2.58 MPa, and WHSV of 3.6 h^{-1}.

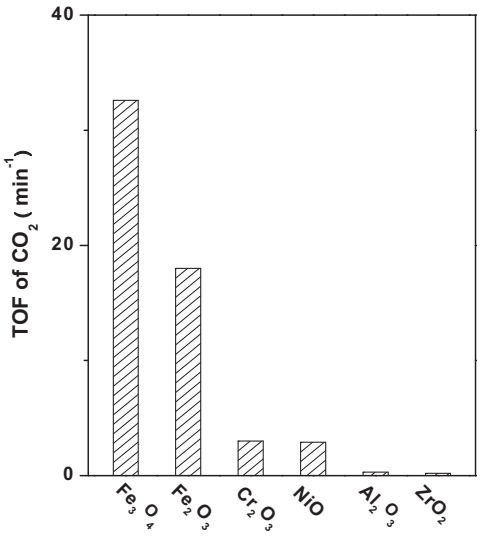

Fig. 5. TOFs of CO_2 in APR of 5 wt.% EG over supported Pd catalysts at 498 K, 2.58 MPa, WHSV of 36.1 h^{-1} for Fe_3O_4-, Fe_2O_3-, Cr_2O_3-, and NiO-supported catalysts, 3.6 h^{-1} for Al_2O_3- and ZrO_2-supported catalysts, and after 6 h on stream.

Table 2
Comparison of catalytic properties over Pd catalysts supported on different metal oxides in APR of 5 wt.% EG at 498 K, 2.58 MPa, WHSV of 3.6 h^{-1}, and after 6 h on stream.

Catalyst	Pd/Fe_3O_4	Pd/Fe_2O_3	Pd/Cr_2O_3	Pd/NiO
Conversion (%)	101.1	51.6	52.3	61.8
Conv. to gas (%)	99.6	41.8	40.1	50.0
H_2 sel. (%)	94.2	96.0	97.5	15.6
Alkane sel. (%)	0.33	0.29	0.28	54.7
Gas products (mol.%)				
H_2	70.2	70.4	70.9	28.5
CO_2	29.5	29.2	28.3	32.9
CO	0.24	0.10	0.68	0.00
Methane	0.10	0.08	0.09	37.2
Ethane	0.00	0.00	0.00	1.10
Propane	0.00	0.00	0.00	0.17
Butane	0.00	0.00	0.00	0.02
Liquid products (mol.%, excluding unconverted EG)				
Methanol	88.8	97.7	83.2	84.3
Ethanol	11.1	2.30	16.5	15.4
Acetone	0.10	0.00	0.20	0.20
2-Propanol	0.00	0.00	0.02	0.10

For the Pd/Fe_2O_3, Pd/NiO, and Pd/Cr_2O_3 catalysts showing appreciable APR activities, the selectivities to H_2 and alkanes as well as gas and liquid product distributions under the same reaction conditions are presented in Table 2. Although the Pd/NiO catalyst displayed higher conversion of EG to gas products than other two catalysts, the selectivity to H_2 was only 16%, while the selectivities to H_2 over the Pd/Fe_2O_3 and Pd/Cr_2O_3 catalysts were as high as 96.0% and 97.5%, respectively. According to Musolino et al. [28], NiO in the Pd/NiO precursor can be reduced to the metallic state at 512 K, which is close to the reduction temperature used here to activate the catalysts. Metallic Ni is an excellent catalyst for the methanation reaction that consumes H_2 [31], resulting in lower selectivity to H_2 but higher selectivity to alkanes on the Pd/NiO catalyst. On the other hand, Fe_2O_3 [18] and Cr_2O_3 [32] were beneficial for the WGS reaction that generates H_2. However, Fig. 6 shows that the Pd/Cr_2O_3 catalyst suffered from rapid deactivation: it lost about a half of its initial activity at 8 h on stream, which could be caused by the instability of the Cr_2O_3 structure in the aqueous environ-

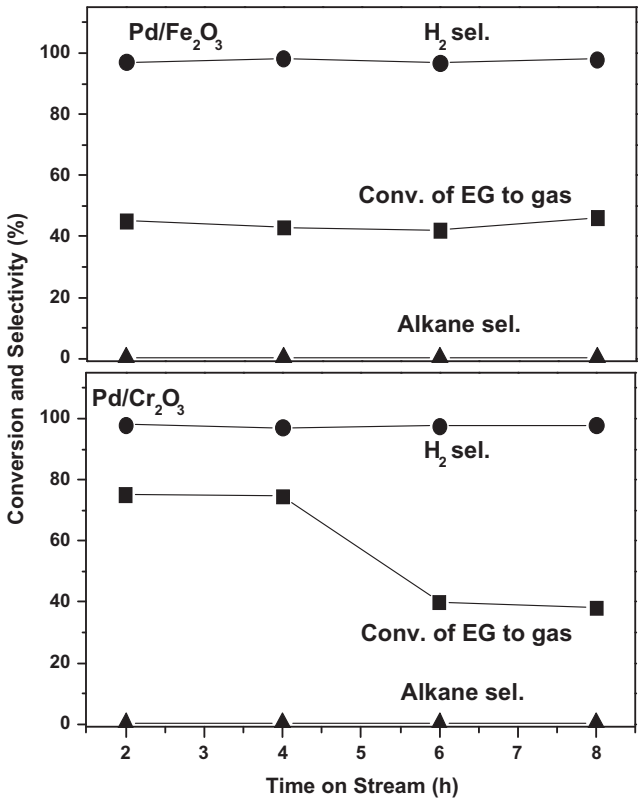

Fig. 6. A comparison of the catalytic performances of the Pd/Fe_2O_3 and Pd/Cr_2O_3 catalysts during 8 h on stream in APR of 5 wt.% EG at 498 K, 2.58 MPa, and WHSV of 3.6 h^{-1}.

ment [33]. Although the initial conversion of EG of the Pd/Fe_2O_3 catalyst was lower than that of the Pd/Cr_2O_3 catalyst, it was more stable. During the same time span, the Pd/Fe_2O_3 catalyst essentially remained its initial activity. Thus, as far as the activity, selectivity, and stability are concerned, Pd/Fe_2O_3 is the most suitable catalyst for APR of EG to H_2 among the supported Pd catalysts prepared by IWI.

The catalytic performance of the Pd/Fe_3O_4 catalyst prepared by co-precipitation was also presented in Fig. 5 and Table 2. It is evident that the APR activity of the Pd/Fe_2O_3 catalyst was far inferior to that of the Pd/Fe_3O_4 catalyst, while the selectivity to H_2 on the latter was only slightly lower under the same reaction conditions. On the Pd/Fe_3O_4 catalyst, the conversion of EG to gas products and selectivity to H_2 could achieve 99.6% and 94.2%, respectively. In a control experiment, since Fig. 2 indicates that magnetite is formed by reduction of $Fe(OH)_x$ at 694 K, we synthesized this magnetite and used it to support Pd by IWI in the way identical to that of the Pd/Fe_2O_3 catalyst. The conversion of EG to gas products on the IWI-derived Pd/Fe_3O_4 catalyst was only 42.0% under the same reaction conditions, unequivocally demonstrating that co-precipitation is more effective than IWI in preparing iron oxide-supported Pd catalyst for APR of EG to H_2.

Table 3 summarizes the intrinsic activities of the Pd/Fe_3O_4 and Pd/Fe_2O_3 catalysts. The absence of transport limitations under the reaction conditions specified in Table 3 was verified following the method proposed by Koros and Nowak [34]. It has been claimed that the reaction rate per gram of catalyst is proportional to S, the number of active sites per unit volume of the reactor, in the absence of any transport limitations. Thus, for the Pd/Fe_3O_4 catalyst, the reaction rate per gram of catalyst should remain constant at various catalyst weights in the kinetically controlled regime. As shown in Fig. 7, the H_2 production rates per gram of the Pd/Fe_3O_4 catalyst, which exhibited the highest activity, were almost identical irrespective of the weight of the catalyst used, strongly indicating that the data in Table 3 as well as in Fig. 5 are intrinsic.

Table 3 shows that in compliance with the results at high conversions, the conversion of EG to gas products on the Pd/Fe_3O_4 catalyst was about 3.2 times of that on the Pd/Fe_2O_3 catalyst. When using the Pd/Fe_3O_4 catalyst in the APR reaction, the production rates of H_2 and CO_2 were accelerated, while the production rates of CO and alkanes were suppressed. It is worth noting that on the Pd/Fe_3O_4 catalyst the production rate of H_2 amounted to 9.21 mmol min^{-1} g_{Pd}^{-1}, corresponding to a H_2 production rate of $\sim$ 700 μmol $cm_{reactor}^{-3}$ min^{-1}. According to Cortright et al. [5], such a H_2 production rate is sufficient to sustain a 1 kW fuel cell assuming 50% efficiency if a 1-l capacity reformer is used.

The higher conversion and production rates of H_2 and CO_2 were not caused exclusively by the higher dispersion of Pd nanoparticles on the Pd/Fe_3O_4 catalyst leading to higher S_{act}. Table 3 shows that the intrinsic activities of the Pd/Fe_3O_4 catalyst expressed as the TOFs of H_2 and CO_2 were also dramatically improved, indicating that the active sites on the Pd/Fe_3O_4 catalyst are not the same as those on the Pd/Fe_2O_3 catalyst. The TOF of H_2 on the Pd/Fe_3O_4 catalyst was 109 min^{-1}, which was substantially higher than the best value (60.1 min^{-1}) ever reported in the literature obtained on a Pd/Fe_2O_3 catalyst prepared by IWI [9], and 48.8 min^{-1} obtained on our

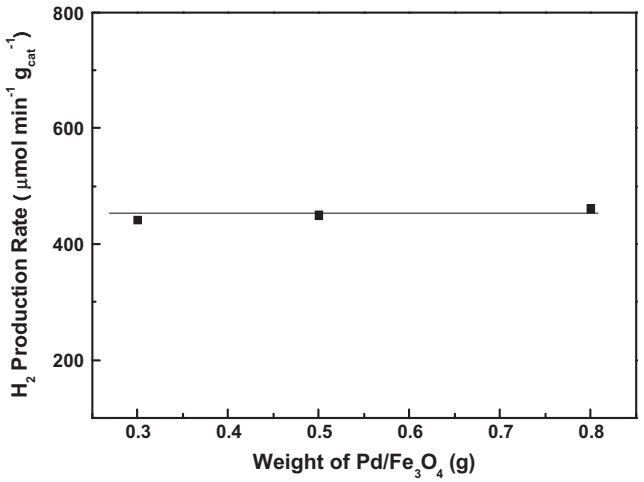

Fig. 7. H_2 production rate per gram of catalyst as a function of the weight of Pd/Fe_3O_4 used in APR of 5 wt.% EG at 498 K, 2.58 MPa, and WHSV of 36.1 h^{-1}.

Table 3
Kinetic results of APR of 5 wt.% EG on the Pd/Fe_3O_4 and Pd/Fe_2O_3 catalysts at 498 K, 2.58 MPa, WHSV of 36.1 h^{-1}, and after 6 h on stream.

Catalyst	Conv. to gas (%)	Production rate $\left(\text{mmol min}^{-1}\ g_{Pd}^{-1}\right)$/TOF ($min^{-1}$)				Sel. (%)	
		H_2	CO_2	CO	CH_4	H_2	Alkane
Pd/Fe_3O_4	14.4	9.21/109	2.76/32.6	9.99×10^{-3}/0.12	8.29×10^{-4}/9.8×10^{-3}	133	0.03
Pd/Fe_2O_3	4.4	2.16/48.8	0.80/18.0	1.90×10^{-2}/0.43	8.59×10^{-4}/1.9×10^{-2}	105	0.1

Pd/Fe_2O_3 catalyst also prepared by IWI. The lower TOF of H_2 on our Pd/Fe_2O_3 catalyst than that on the literature catalyst may be due to experimental differences between different laboratories.

According to Shabaker et al. [10], the ratios of the partial pressures Q_P ($Q_P = P_{CO2}P_{H2}/P_{CO}$) under reaction conditions indicated in Table 3 were calculated, and the quotient Q_P/K_{WGS} ($K_{WGS} = P_{CO2}P_{H2}/P_{CO}a_{H2O}$) denoting the extent of the WGS reaction was determined to be 0.25 and 0.067 for the Pd/Fe_3O_4 and Pd/Fe_2O_3 catalysts, respectively. The small Q_P/K_{WGS} ratio for the Pd/Fe_2O_3 catalyst implies that the WGS reaction was far from equilibrium, while the extent of the WGS reaction was greatly enhanced when using the Pd/Fe_3O_4 catalyst. A good APR catalyst should be active both in the cleavage of the C–C bond and in the WGS reaction [11], and the rate-determining step for APR on Pd catalyst could be the WGS reaction [9], which may be rationalized by previous experimental [35–37] and theoretical work [38,39] that water does not dissociate on the clean Pd{1 1 1} surface. The WGS reaction not only produces more H_2 from EG but also eliminates adsorbed CO from the catalyst surface, or high surface coverage of CO would lead to low catalytic activity [9].

For high-temperature WGS reaction, magnetite rather than hematite is the active phase and generally obeys the multi-step redox or regenerative mechanism [40,41]. Boreskov demonstrated that the Fe^{2+} and Fe^{3+} ions located in octahedral sites in the magnetite-based structure function as a redox couple and that magnetite-based catalysts can be highly effective for the complete dissociation of water into H_2 and adsorbed O under reaction conditions. Water dissociation causes the oxidation of the octahedral Fe^{2+} to Fe^{3+} and liberates H_2. The oxidized iron centers may subsequently be reduced by CO thereby producing CO_2 to complete the catalytic cycle [42]. Among these steps, Keiski et al. indicated that CO adsorption is one of the rate-determining steps based on the stationary and transient kinetics of the WGS reaction over an industrial ferrochrome catalyst [43]. Using TPD, IRAS, and HREELS, Lemire et al. examined the adsorption of CO and water on Fe_3O_4(1 1 1) films and evidenced that water readily dissociates and blocks the Fe^{3+} step sites which bind most strongly with CO [44]. For supported metal catalysts, the WGS reaction generally occurs in a bifunctional manner, with the participation of both the dispersed metallic phase and the support. The role of noble metal is most probably restricted to CO adsorption and supply to the metal–support interface to form CO_2 [15]. It is well known that Pd readily adsorbs CO [45]. According to our XRD, H_2–TPR, and BET results, in the Pd/Fe_3O_4 catalyst the iron oxide support was in the form of magnetite with large BET surface area, and Pd nanoparticles were less than 3 nm in diameter. In the Pd/Fe_2O_3 catalyst, the iron oxide support was mainly in the form of hematite with small BET surface area, and only weak diffraction peaks of magnetite were present. The Pd nanoparticles in this catalyst were about 10 nm in diameter. Therefore, in the Pd/Fe_3O_4 catalyst a stronger cooperative effect between Pd and magnetite than that in the Pd/Fe_2O_3 catalyst is expected, thus resulting in exceptionally higher TOFs of H_2 and CO_2 and consequently a higher Q_p on the Pd/Fe_3O_4 catalyst prepared by the co-precipitation method. This argument is directly justified by the much higher WGS activity over the Pd/Fe_3O_4 catalyst than that over the Pd/Fe_2O_3 evaluated on a separate WGS reactor described previously [46]. In Fig. 8, it is found that under the same WGS reaction conditions, the conversion of CO on the Pd/Fe_2O_3 catalyst was 15%, whereas it was as high as 91% on the Pd/Fe_3O_4 catalyst.

3.3. Catalytic stability

For the Pd/Fe_2O_3 catalyst, Huber et al. reported that although the catalyst had the highest TOF of H_2 among the catalysts tested in APR of EG, it lost 50% of its activity after the reaction temperature was cycled from 453 K to 483 K and back, staying at each temperature for 15 h. They pointed out that future catalyst development work should focus on how to prepare more stable PdFe catalyst [9]. Thus, it will be of practical significance to know whether the Pd/Fe_3O_4 catalyst prepared by co-precipitation is also stable in APR of EG to H_2.

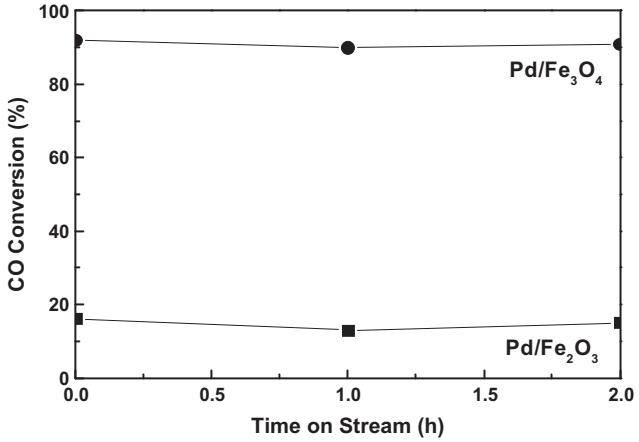

Fig. 8. CO conversions over the Pd/Fe_3O_4 and Pd/Fe_2O_3 catalysts at 498 K, atmospheric pressure, feed composition of 10.6% CO and 29.3% H_2O (balance N_2), and gas hourly space velocity of 15,000 h^{-1}.

Fig. 9 presents the catalytic performance of the Pd/Fe_3O_4 catalyst versus time-on-stream during APR of EG. It should be mentioned that the WHSV of 3.6 h^{-1} used here is the experimentally determined turning point at which the conversion of EG to gas products just reached 100%. After the first 50 h on stream, the conversion of EG to gas products only dropped slightly from 100% to 97%. During the next 50 h on stream, the catalyst underwent a relatively obvious deactivation, approaching a steady-state conversion of EG to gas products of approximately 80%. It is thus clear that co-precipitation is a highly effective method to answer the question raised by Huber et al. [9]. Moreover, during 130 h on stream, the selectivity to H_2 increased gradually from ca. 92% to 100%, and the selectivity to alkanes was always below 0.1%. The increase in selectivity to H_2 with aging may be due to the incomplete reforming reactions. Considering its lower cost than Pt and its higher stability and selectivity to H_2 than Ni-based catalysts [25], the Pd/Fe_3O_4 catalyst is a very promising high-performance candidate for converting EG to H_2.

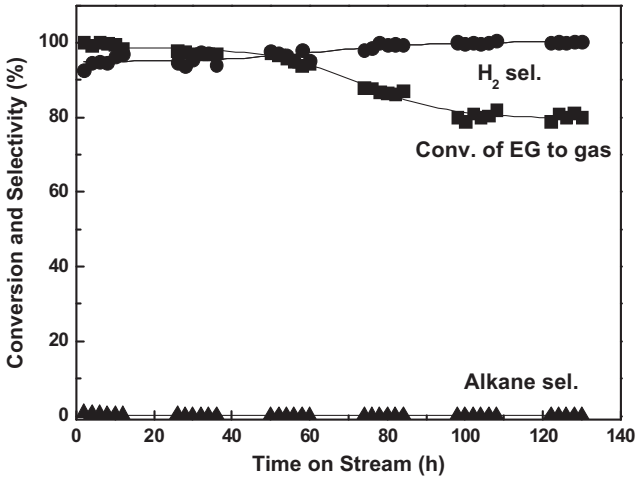

Fig. 9. The catalytic performance of the Pd/Fe_3O_4 catalyst during 130 h on stream in APR of 5 wt.% EG at 498 K, 2.58 MPa, and WHSV of 3.6 h^{-1}.

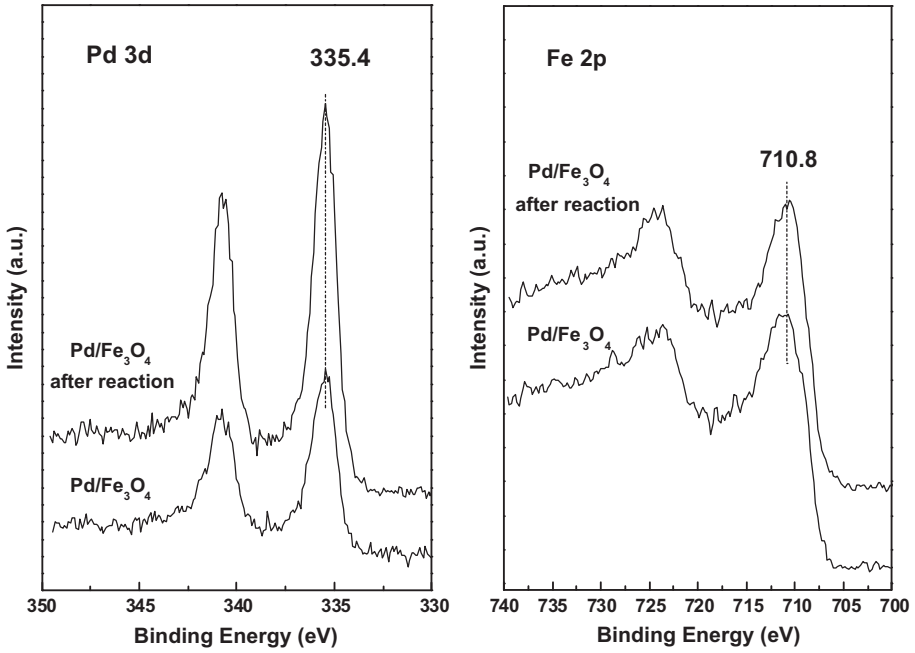

Fig. 10. Pd 3d and Fe 2p spectra of the Pd/Fe_3O_4 catalyst before and after 130 h on stream in APR of 5 wt.% EG at 498 K, 2.58 MPa, and WHSV of 3.6 h^{-1}.

To better understand the change in the catalytic performance in the stability test, the Pd/Fe_3O_4 catalyst after 130 h on stream was systematically characterized. Chemical analysis revealed that the concentrations of Pd and Fe dissolved in the liquid products after 130 h on stream were both less than 1.0 ppm, verifying that the activity loss should not be induced by the leaching of the active phase and the support. Pd 3d and Fe 2p spectra shown in Fig. 10 disclosed that after the stability test, the Pd species was still in the metallic state with the Pd $3d_{5/2}$ BE of 335.4 eV [47], and the Fe species was still in the form of magnetite with the Fe $2p_{3/2}$ BE of ca. 710.8 eV [48]. For comparison, on Ni-based catalysts the oxidation of metallic Ni occurred during APR of EG, which can be an important reason for the deactivation of Ni-based APR catalysts [25,49]. In addition, the surface Pd/Fe atomic ratio derived from Fig. 10 increased from 0.05 to 0.11 after 130 h on stream.

The XRD pattern of the Pd/Fe_3O_4 catalyst after 130 h on stream is also illustrated in Fig. 1. When compared to the as-reduced Pd/Fe_3O_4 catalyst, the diffraction peaks due to magnetite were sharpened, which signifies the sintering of magnetite. According to the Scherrer equation, the crystallite size of magnetite in the Pd/Fe_3O_4 catalyst after reaction was 21 nm, which is larger than the value of 11 nm in the as-reduced Pd/Fe_3O_4 catalyst. After the stability test, there was still no diffraction peak of metallic Pd (Fig. 1), signifying again the strong interaction between Pd and magnetite in the Pd/Fe_3O_4 catalyst. So, the increased surface Pd/Fe ratio after 130 h on stream obtained above can be rationalized by the decreased dispersity of magnetite. However, in the TEM image of the Pd/Fe_3O_4 catalyst after the stability test (Fig. 4d), we observed some Pd nanoparticles with dimension of ca. 5 nm, possibly due to the sintering of Pd nanoparticles loosely bonding with magnetite. Based on these results, we tentatively attribute the 20% deactivation of the Pd/Fe_3O_4 catalyst after 130 h on stream to the sintering of magnetite and some weakly bound Pd nanoparticles with magnetite during APR of EG.

4. Conclusion

The preparation method has a profound effect on the catalytic performance of iron oxide-supported Pd catalysts for APR of EG to H_2. On the Pd/Fe_3O_4 catalyst prepared by the co-precipitation method, the TOF of H_2 in APR of EG represents the highest value ever reported in open literature. Based on the characterizations and literature works, we suggest a synergistic mechanism on the Pd/Fe_3O_4 catalyst involving small Pd nanoparticles and magnetite which effectively promotes the WGS reaction that is believed as the rate-determining step for APR of EG over Pd-based catalysts. Moreover, the Pd/Fe_3O_4 catalyst retained 80% of its initial APR activity after reaching the steady-state. Thus, the Pd/Fe_3O_4 catalyst prepared by the co-precipitation method can be regarded as the most promising candidate thus far for the APR of biomass-derived oxygenates to H_2 for fuel cell applications.

Acknowledgments

This work was supported by the National Basic Research Program of China (2006CB202502), the Program of New Century Excellent Talents in Universities (NCET-08-0126), the Fok Ying Tong Education Foundation (104022), the NSF of China (20673025, 20703011, 20803011, J0730419), and the Science and Technology Commission of Shanghai Municipality (06JC14009, 08DZ2270500, 09ZR1402300). The authors also thank Ms. Rui Dai for collecting the reaction data, Dr. Songhai Xie for his assistance in TEM and XPS characterizations, and Prof. Kangnian Fan for his valuable help in writing this paper.

References

[1] D. Pimentel, G. Rodrigues, T. Wang, R. Abrams, K. Goldberg, H. Staecker, E. Ma, L. Brueckner, L. Trovato, C. Chow, U. Govindarajulu, S. Boerke, BioScience 44 (1994) 536.
[2] M. Ishida, K. Otsuka, S. Takenaka, I. Yamanaka, J. Chem. Technol. Biotechnol. 80 (2005) 281.
[3] D. Preti, S. Squarcialupi, G. Fachinetti, Angew. Chem. Int. Ed. 48 (2009) 4763.
[4] J. Turner, G. Sverdrup, M.K. Mann, P.C. Maness, B. Kroposki, M. Ghirardi, R.J. Evans, D. Blake, Int. J. Energy Res. 32 (2008) 379.
[5] R.D. Cortright, R.R. Davda, J.A. Dumesic, Nature 418 (2002) 964.
[6] G.W. Huber, J.W. Shabaker, J.A. Dumesic, Science 300 (2003) 2075.
[7] R.R. Davda, J.W. Shabaker, G.W. Huber, R.D. Cortright, J.A. Dumesic, Appl. Catal. B 43 (2003) 13.
[8] J.W. Shabaker, D.A. Simonetti, R.D. Cortright, J.A. Dumesic, J. Catal. 231 (2005) 67.

[9] G.W. Huber, J.W. Shabaker, S.T. Evans, J.A. Dumesic, Appl. Catal. B 62 (2006) 226.
[10] J.W. Shabaker, R.R. Davda, G.W. Huber, R.D. Cortright, J.A. Dumesic, J. Catal. 215 (2003) 344.
[11] R.R. Davda, J.W. Shabaker, G.W. Huber, R.D. Cortright, J.A. Dumesic, Appl. Catal. B 56 (2005) 171.
[12] J.H. Sinfelt, D.J.C. Yates, J. Catal. 8 (1967) 82.
[13] D.C. Grenoble, M.M. Estadt, D.F. Ollis, J. Catal. 67 (1981) 90.
[14] J.A. Rodriguez, P. Liu, J. Hrbek, J. Evans, M. Pérez, Angew. Chem. Int. Ed. 46 (2007) 1329.
[15] P. Panagiotopoulou, D.I. Kondarides, J. Catal. 225 (2004) 327.
[16] M. Haruta, J. Nanopart. Res. 5 (2003) 3.
[17] S. Zhao, R.J. Gorte, Catal. Lett. 92 (2004) 75.
[18] X. Wang, R.J. Gorte, Appl. Catal. A 247 (2003) 157.
[19] F. Schüth, M. Hesse, K.K. Unger, in: G. Ertl, H. Knözinger, F. Schüth, J. Weitkamp (Eds.), Handbook of Heterogeneous Catalysis, Wiley-VCH, Weinheim, 2008, p. 100.
[20] F. Liu, S.P. Xu, L. Cao, Y. Chi, T. Zhang, D.F. Xue, J. Phys. Chem. C 111 (2007) 7396.
[21] G. Neri, G. Rizzo, L. De Luca, A. Donato, M.G. Musolino, R. Pietropaolo, Appl. Catal. A 356 (2009) 113.
[22] B. Bridier, N. López, J. Pérez-Ramírez, J. Catal. 269 (2010) 80.
[23] B.T. Qiao, L.Q. Liu, J. Zhang, Y.Q. Deng, J. Catal. 261 (2009) 241.
[24] H. Dropsch, M. Baerns, Appl. Catal. A: Gen. 158 (1997) 163.
[25] J.W. Shabaker, G.W. Huber, J.A. Dumesic, J. Catal. 222 (2004) 180.
[26] G. Munteanu, L. Ilieva, D. Andreeva, Thermochim. Acta 291 (1997) 171.
[27] F.W. Chang, L.S. Roselin, T.C. Ou, Appl. Catal. A 334 (2008) 147.
[28] M.G. Musolino, C. Busacca, F. Mauriello, R. Pietropaolo, Appl. Catal. A 379 (2010) 77.
[29] M. Kruk, M. Jaroniec, Chem. Mater. 13 (2001) 3169.
[30] J.W. Shabaker, G.W. Huber, R.R. Davda, R.D. Cortright, J.A. Dumesic, Catal. Lett. 88 (2003) 1.
[31] M.A. Vannice, J. Catal. 50 (1977) 228.
[32] L. Ma, B. Gong, T. Tran, M.S. Wainwright, Catal. Today 63 (2000) 499.
[33] X.L. Hong, S.Z. Ren, Int. J. Hydrogen Energy 33 (2008) 700.
[34] R.M. Koros, E.J. Nowak, Chem. Eng. Sci. 22 (1967) 470.
[35] X.Y. Zhu, J. White, M. Wolf, E. Hasselbrink, G. Ertl, J. Phys. Chem. 95 (1991) 8393.
[36] C. Clay, L. Cummings, A. Hodgson, Surf. Sci. 601 (2007) 562.
[37] M.J. Gladys, A.A. El Zein, A. Mikkelsen, J.N. Anderson, G. Held, Surf. Sci. 602 (2008) 3540.
[38] A. Michaelides, A. Alavi, D.A. King, Phys. Rev. B 69 (2004) 113404.
[39] G.S. Karlberg, Phys. Rev. B 74 (2006) 153414.
[40] C. Rhodes, G.J. Hutchings, A.M. Ward, Catal. Today 23 (1995) 43.
[41] C. Ratnasamy, J.P. Wagner, Catal. Rev. 51 (2009) 325.
[42] G.K. Boreskov, Kinet. Katal. 11 (1970) 374.
[43] R.L. Keiski, T. Salmi, P. Niemistö, J. Ainassaari, V.J. Pohjola, Appl. Catal. A 137 (1996) 349.
[44] C. Lemire, R. Meyer, V.E. Henrich, Sh. Shaikhutdinov, H.J. Freund, Surf. Sci. 572 (2004) 103.
[45] H. Conrad, G. Ertl, J. Koch, E.E. Latta, Surf. Sci. 43 (1974) 462.
[46] P.J. Guo, L.F. Chen, Q.Y. Yang, M.H. Qiao, H. Li, H.X. Li, H.L. Xu, K.N. Fan, Int. J. Hydrogen Energy 34 (2009) 2361.
[47] P.M.Th.M. van Attekum, J.M. Trooster, Phys. Rev. B 20 (1979) 2335.
[48] T. Choudhury, S.O. Saied, J.L. Sullivan, A.M. Abbot, J. Phys. D 22 (1989) 1185.
[49] L.J. Zhu, P.J. Guo, X.W. Chu, S.R. Yan, M.H. Qiao, K.N. Fan, X.X. Zhang, B.N. Zong, Green Chem. 10 (2008) 1323.